CHEMISTRY OF MATERIALS
Article

Chem. Mater. **2010,** *22,* 1155–1163 1155
DOI:10.1021/cm902483a

Strongly Correlated Properties and Enhanced Thermoelectric Response in $Ca_3Co_{4-x}M_xO_9$ (M = Fe, Mn, and Cu)†

Yang Wang,*[,‡,§] Yu Sui,[§,∥] Peng Ren,[‡] Lan Wang,[‡] Xianjie Wang,[§] Wenhui Su,[§] and Hongjin Fan*[,‡]

[‡]*Division of Physics and Applied Physics, School of Physical and Mathematical Sciences, Nanyang Technological University, 21 Nanyang Link, 637371 Singapore,* [§]*Center for Condensed Matter Science and Technology (CCMST), Department of Physics, Harbin Institute of Technology, Harbin 150001, People's Republic of China, and* [∥]*International Center for Materials Physics, Academia Sinica, Shenyang 110015, People's Republic of China*

Received August 13, 2009. Revised Manuscript Received September 24, 2009

We report the strongly correlated, electrical transport, magnetic, and thermoelectric properties of a series of Fe, Mn, and Cu doped $Ca_3Co_4O_9$. The results indicate that Fe/Mn substitutes for Co in CoO_2 layers whereas Cu substitutes for Co in Ca_2CoO_3 layers. Because of the different doping sites, the electronic correlations increase remarkably in Fe and Mn doped series while remaining unchanged in Cu doped series. Correspondingly, the transport mechanism, magnetic properties, and some characteristic parameters along with transition temperatures all exhibit two distinct evolutions for Fe/Mn doping and Cu doping. The thermoelectric characteristics are improved in each series. Nevertheless, the improvement of thermoelectric performance is most significant in Fe doped samples due to the unexpected changes in thermopower and resistivity. The unusual thermopower behavior can be well described by the variations of electronic correlation. Possible approaches for further improvement of the thermoelectric performance in $Ca_3Co_4O_9$ and other relevant strongly correlated systems are also proposed at the end.

Introduction

Since the discovery of large thermoelectric response in $NaCo_2O_4$ and $Ca_3Co_4O_9$[1,2] and especially the superconductivity in hydrated $Na_{0.35}CoO_2$,[3] such layered cobaltites have attracted increasing attention. As electron strongly correlated systems, these cobaltites exhibit unusual thermoelectric properties, namely, the coexistence of a large thermopower and a low resistivity, which makes these compounds an attractive candidate for thermoelectric application. Usually, a large thermopower is associated with low carrier concentration, and the thermoelectric properties are optimized for materials with a typical carrier density of 10^{19} cm^{-3}.[4] However, in $NaCo_2O_4$ and $Ca_3Co_4O_9$, the carrier concentration can reach 10^{21} cm^{-3},[1,5] and these compounds yet show a thermopower comparable to that of the usual low-carrier-concentration thermoelectric materials. Obviously, their thermopower is not simply determined by carrier concentration. To elucidate the source of large thermopower along with low resistivity in the cobaltite systems, several mechanisms have been proposed.[6−12] In general, the unusual thermoelectric response may involve spin and orbital degeneracies (configurational entropy),[6−8] spin and charge frustrations,[1,9] enhanced effective mass in the vicinity of Mott metal−insulator transition,[10] or strong electronic correlations.[11,12] The considerable electronic specific heat coefficient γ (~48 mJ mol^{-1} K^{-2} for $NaCo_2O_4$ and ~93 mJ mol^{-1} K^{-2} for $Ca_3Co_4O_9$)[11,12] indicates that the strong electronic correlations and thus large electronic effective mass exist in these cobaltites.

In addition to the thermoelectric and strongly correlated properties, the transport mechanism and magnetic properties of these misfit-layered cobaltites are also complicated and remain unclear. For example, of $Ca_3Co_4O_9$, although it is considered that as temperature increases $Ca_3Co_4O_9$ undergoes the evolution from a low temperature

† Accepted as part of the 2010 "Materials Chemistry of Energy Conversion Special Issue".

*Corresponding authors. E-mail: wang_yang@ntu.edu.sg (W.Y.); fanhj@ntu.edu.sg (H.J.F.).

(1) Terasaki, I.; Sasago, Y.; Uchinokura, K. *Phys. Rev. B* **1997**, *56*, R12685.
(2) Masset, A. C.; Michel, C.; Maignan, A.; Hervieu, M.; Toulemonde, O.; Studer, F.; Reveau, B.; Hejtmanek, J. *Phys. Rev. B* **2000**, *62*, 166.
(3) Takada, K.; Sakurai, H.; Takayama-Muromachi, E.; Izumi, F.; Dilanian, R. A.; Sasaki, T. *Nature* **2003**, *422*, 53.
(4) Mahan, G. D. *Solid State Phys.* **1998**, *51*, 81.
(5) Zhao, B. C.; Sun, Y. P.; Song, W. H. *J. Appl. Phys.* **2006**, *99*, 073906.
(6) Koshibae, W.; Tsutsui, K.; Maekawa, S. *Phys. Rev. B* **2000**, *62*, 6869.
(7) Koshibae, W.; Maekawa, S. *Phys. Rev. Lett.* **2001**, *87*, 236603.
(8) Wang, Y.; Rogado, N. S.; Cava, R. J.; Ong, N. P. *Nature* **2003**, *423*, 425.
(9) Motrunich, O. I.; Lee, P. A. *Phys. Rev. B* **2004**, *69*, 214516.
(10) Pálsson, G.; Kotliar, G. *Phys. Rev. Lett.* **1998**, *80*, 4775.
(11) Limelette, P.; Hardy, V.; Auban-Senzier, P.; Jérome, D.; Flahaut, D.; Hébert, S.; Frésard, R.; Simon, Ch.; Noudem, J.; Maignan, A. *Phys. Rev. B* **2005**, *71*, 233108.
(12) Ando, Y.; Miyamoto, N.; Segawa, K.; Kawata, T.; Terasaki, I. *Phys. Rev. B* **1999**, *60*, 10580.

Published on Web 10/14/2009

Table 1. Density, Oxygen Content, Room-Temperature Transport and Thermoelectric Parameters, Electronic Correlated Characteristic Parameters, and Transition Temperatures for All the Samples

		Fe		Mn		Cu	
	$x = 0$	$x = 0.05$	$x = 0.1$	$x = 0.05$	$x = 0.1$	$x = 0.05$	$x = 0.1$
d (g/cm^3)	3.861(3)	3.843(5)	3.856(3)	3.871(4)	3.852(5)	3.867(3)	3.878(5)
δ[a]	0.35(2)	0.36(3)	0.36(2)	0.37(3)	0.36(3)	0.35(3)	0.36(2)
ρ (300 K) (mΩ cm)	18.4	16.7	16.2	22.3	25.2	14.4	11.8
S (300K) (μV/K)	124.1	156.2	175.6	138.5	154.4	112.9	101.3
κ (300K) (Wm^{1-}K^{-1})	2.87	2.53	2.23	2.51	2.37	2.32	1.96
P (300 K) (μW m^{-1} K^{-2})	83.7	146.1	190.3	86.2	94.6	88.5	87.0
ZT (300 K)	0.009	0.017	0.026	0.011	0.013	0.012	0.014
n (300 K) (10^{20} cm^{-3})	4.30	4.52	4.66	4.21	4.08	4.59	4.72
m^*/m_0	12.6	14.3	15.2	13.5	14.1	12.4	12.7
A/A_0[b]	1	1.46	1.78	1.21	1.35	0.97	0.98
T_{MI} (K)	80	75	71	77	74	81	80
T^* (K)	195 ± 2	187 ± 2	168 ± 2	191 ± 2	176 ± 2	195 ± 2	196 ± 2
T_S^* (K)	113.5	107.2	104.1	110.8	109.2	113.0	113.2
ΔE (meV)	1.30	1.53	1.91	1.43	1.67	1.32	1.33

[a] δ denotes the excess oxygen in the expression "$Ca_3Co_4O_{9+\delta}$". [b] A_0 is the Fermi liquid transport coefficient A of the $Ca_3Co_4O_9$ parent.

insulator to a strongly correlated Fermi liquid to an incoherent metal and finally to a semiconductor at elevated temperature,[11] recently a spin dependent scattering behavior in addition to a shadowed metallic-like conduction over a large temperature range was observed.[13] Susceptibility measurements indicate two magnetic transitions around 19 K and 380 K, respectively. The former is a ferrimagnetic transition, and the latter is probably induced by a spin state transition.[2,14−16] Also, it was observed that the short-range incommensurate spin-density-wave (IC-SDW) ordering appears below ~100 K, whereas the long-range IC-SDW ordering is complete below ~30 K, and the formation of IC-SDW is responsible for the metal−insulator (MI) transition around 80 K.[15,16] Particularly, it was found that the ferrimagnetism is caused by the interlayer coupling while the IC-SDW propagates in-plane, suggesting their different origins.[14−16]

These layered cobaltites consist of two alternating structural subsystems and share a common subsystem: CdI_2-type hexagonal CoO_2 layers in which two-dimensional triangular lattices of Co ions are formed by a network of edge-sharing CoO_6 octahedra.[2] The other subsystems are disorder-distributed Na ions in $NaCo_2O_4$[1] and rocksalt-type Ca_2CoO_3 layers in $Ca_3Co_4O_9$,[2] respectively. As a result, these cobaltites show highly anisotropic properties. Charge carrier transport is mainly restricted to the CoO_2 planes, and the carriers can vary over a remarkably wide range by doping so that the effective valence of Co ions can change from Co^{2+} to Co^{4+} in these materials.[17] Therefore, ion-doping may influence the transport, thermoelectric, and magnetic properties evidently.[5,15,18−21] For instance, the substitution of Y or Bi for Ca increases the IC-SDW transition temperature and annihilates the ferrimagnetism in $Ca_3Co_4O_9$;[15] the substitution of Mn or Fe for Co changes the electrical transport characteristics;[19,20] and the substitution of Ti leads to an enhanced spin fluctuation and spin glass behavior.[21] In contrast, the investigations on the effect of doping on the strongly correlated properties are very scanty. It was reported that the substitution of Ca^{2+} for Na^+ has little influence of the electronic correlation in $NaCo_2O_4$,[12] and recently we found that the substitution of Ag^+ for Ca^{2+} can alter the strongly correlated properties of $Ca_3Co_4O_9$ due to chemical pressure.[22] In fact, doping in Co sites of CoO_2 layers may induce more notable variation of electronic correlations, because the CoO_2 layers not only dominate charge carrier conduction but also play an important role in determining electronic structure as revealed by the band calculation that Fermi energy lies in the crystal-field gap of the d states in CoO_2 subsystem.[23] To our knowledge, such studies have not yet been conducted, but they are significant to understand the sources of strong electronic correlation and unusual thermoelectric response. It this paper, we report the effects of substitution of Fe, Mn, and Cu for Co on the strongly correlated properties in $Ca_3Co_4O_9$ and discuss the mechanism of the improvement of thermoelectric response by the transition metal doping.

Experimental Section

Polycrystalline $Ca_3Co_{4-x}M_xO_9$ (M = Fe, Mn, and Cu; $x = 0$, 0.05, and 0.1) samples were prepared by the solid-state reaction method. Reagent grade $CaCO_3$, Co_2O_3, Fe_2O_3, MnO_2, and Cu_2O powders in stoichiometric ratio were mixed thoroughly and calcined in air at 1173 K for 12 h. Then the mixture was reground, pressed into dish-shaped pellets, and sintered at 1223 K for 36 h under an O_2 flow with intermediate grindings.

(13) Limelette, P.; Soret, J. C.; Muguerra, H.; Grebille, D. *Phys. Rev. B* **2008**, *77*, 245123.
(14) Sugiyama, J.; Xia, C.; Tani, T. *Phys. Rev. B* **2003**, *67*, 104410.
(15) Sugiyama, J.; Itahara, H.; Tani, T.; Brewer, J. H.; Ansaldo, E. J. *Phys. Rev. B* **2002**, *66*, 134413.
(16) Sugiyama, J.; Brewer, J. H.; Ansaldo, E. J.; Itahara, H.; Dohmae, K.; Seno, Y.; Xia, C.; Tani, T. *Phys. Rev. B* **2003**, *68*, 134423.
(17) Imada, M.; Fujimori, A.; Tokura, Y. *Rev. Mod. Phys.* **1998**, *70*, 1039.
(18) Wang, Y.; Sui, Y.; Cheng, J. G.; Wang, X. J.; Su, W. H. *J. Phys. D: Appl. Phys.* **2008**, *41*, 045406.
(19) Liu, C. J.; Huang, L. C.; Wang, J. S. *Appl. Phys. Lett.* **2006**, *89*, 204102.
(20) Li, D.; Qin, X. Y.; Gu, Y. J.; Zhang, J. *J. Appl. Phys.* **2006**, *99*, 053709.
(21) Zhao, B. C.; Sun, Y. P.; Lu, W. J.; Zhu, X. B.; Song, W. H. *Phys. Rev. B* **2006**, *74*, 144417.
(22) Wang, Y.; Sui, Y.; Cheng, J. G.; Wang, X. J.; Su, W. H. *J. Phys.: Condens. Matter* **2007**, *19*, 356216.
(23) Asahi, R.; Sugiyama, J.; Tani, T. *Phys. Rev. B* **2002**, *66*, 155103.

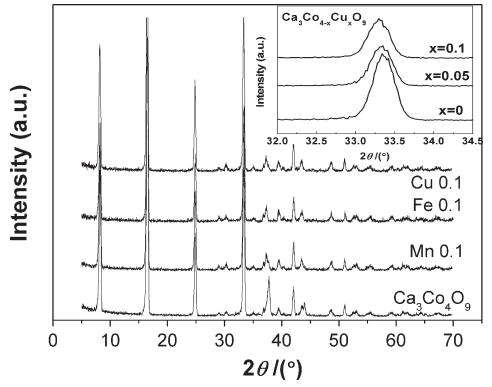

Figure 1. XRD patterns of $Ca_3Co_{4-x}M_xO_9$ ($x = 0.1$) samples. The inset shows magnified (004) peaks of Cu doped samples.

X-ray powder diffraction (XRD) data at room temperature were collected using the XRD diffractometer (D8 Advanced) with Cu Kα ($\lambda = 0.15406$ nm) radiation. The microstructure was observed with a JEOL JSM-6700F scanning electron microscope (SEM). Oxygen content was determined by iodometric titration and thermogravimetry. Note that "$Ca_3Co_4O_9$" is actually an abbreviation of "$Ca_9Co_{12}O_{28}$" or "$[Ca_2CoO_3]_{0.62}$-$[CoO_2]$",[2] so the oxygen content of $Ca_3Co_4O_9$ is about 9.33. As shown in Table 1, the oxygen content of undoped $Ca_3Co_4O_9$ is ~9.35 and increases slightly in doped samples. The density of the samples was determined by the Archimedes method at room temperature, as listed in Table 1. The density values of all samples, d, are ~3.8−3.9 g/cm^2, which are ~78% of that of theoretical fully dense material (4.94 g/cm^3).

Temperature dependence of resistivity, thermopower, specific heat, thermal conductivity, and magnetic measurements were all carried out by using the commercial Quantum Design physical property measurement system (PPMS-9T). Resistivity measurements were performed by the standard four-probe method. Thermopower was calculated by measuring the thermoelectric voltage and the temperature gradient across the sample. Thermal conductivity and specific heat were measured using a steady-state technique in a closed cycle refrigerator pumped down to 10^{-5} Torr. Carrier concentrations were determined by Hall measurements, using the standard five-wire method and conducted by PPMS. First, Hall resistivity ρ_H was measured under a varying magnetic field; then Hall coefficient R_H can be obtained from the slope of $\rho_H - H$ plot. Subsequently the carrier concentration n was calculated from $n = 1/eR_H$.

Results and Discussion

The XRD patterns at room temperature of the sample are shown in Figure 1. The XRD patterns of all the samples agree well with the standard JCPDS card (21-139) and reported data for the $Ca_3Co_4O_9$ structure,[2,24] indicating the formation of single-phase compounds. With M doping, it can be observed that the diffraction peaks shift slightly, mostly owing to the different radii of M ions and Co ions. In the $Ca_3Co_4O_9$ system, the substitution of M for Co can actually take place in either the Ca_2CoO_3 layers or CoO_2 layers.[21,25] In the following

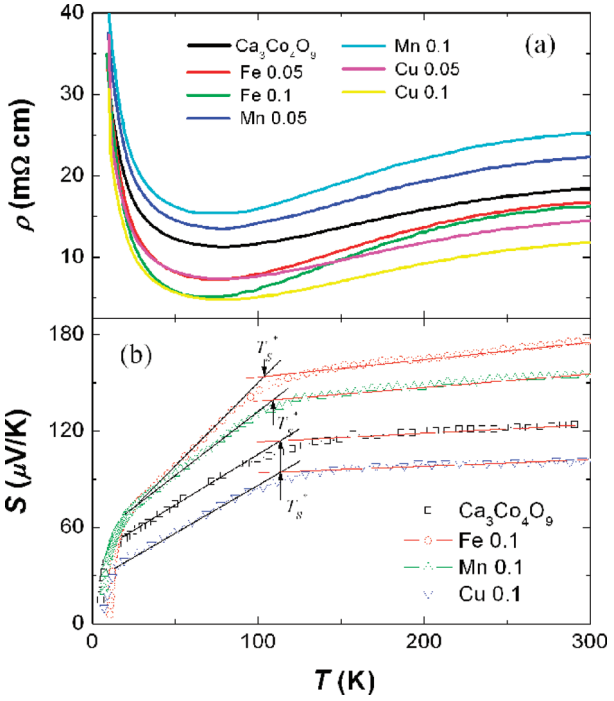

Figure 2. Temperature dependences of (a) resistivity ρ and (b) thermopower S of the samples. The solid lines in the $S-T$ curves are fitted lines as defined in the text. T_S*, marked by arrows, denotes the cross point of the two fitting straight lines.

physical properties analysis, one will see that Fe or Mn ions mainly occupy Co sites in CoO_2 layers whereas Cu ions essentially occupy Co sites in Ca_2CoO_3 layers. The SEM micrograph (see Supporting Information) indicates that the samples are dense, but with light porosity. In addition, although a plate-shaped layered structure is observed, the samples do not exhibit a clear crystallographic anisotropy. This may result from our conventional solid-state reaction fabrication method. Compared with $Ca_3Co_4O_9$ ceramics synthesized by template growth or the hot-pressure method,[26] our samples are not highly textured and have a relative low density and small grain size.

Strongly Correlated Properties. Temperature dependences of resistivity ρ and thermopower S of the samples are shown in Figure 2. Compared with the $Ca_3Co_4O_9$ parent, doping by Fe, Mn, or Cu does not change the shapes of the $\rho-T$ and $S-T$ curves on the whole but changes the values of ρ and S obviously. It can be found that Fe doping decreases ρ but increases S; Mn doping increases ρ and S simultaneously; and Cu doping reduces ρ and S simultaneously. The variations of ρ can be explained by the change in carrier concentration of the system. In the $Ca_3Co_4O_9$ system, the majority of the charge carriers are hole-type, as confirmed by the positive values of the Hall coefficient and thermopower.[11] Co ions have three types of valences: Co^{2+}, Co^{3+}, and Co^{4+}, and the average valence of Co is between +3 and +4 depending

(24) Mikami, M.; Ohtsuka, S.; Yoshimura, M.; Mori, Y.; Sasaki, T.; Funahashi, R.; Shikano, M. *Jpn. J. Appl. Phys.* **2003**, *42*(Part 1), 3549.
(25) Yao, Q.; Wang, D. L.; Chen, L. D.; Shi, X.; Zhou, M. *J. Appl. Phys.* **2005**, *97*, 103905.
(26) Itahara, H.; Seo, W. S.; Lee, S.; Nozaki, H.; Tani, T.; Koumoto, K. *J. Am. Chem. Soc.* **2005**, *127*, 6367. Masuda, Y.; Nagahama, D.; Itahara, H.; Tani, T.; Seo, W. S.; Koumoto, K. *J. Mater. Chem.* **2003**, *13*, 1094. Xu, G. J.; Funahashi, R.; Shikano, M.; Pu, Q. R.; Liu, B. *Solid State Commun.* **2002**, *124*, 73.

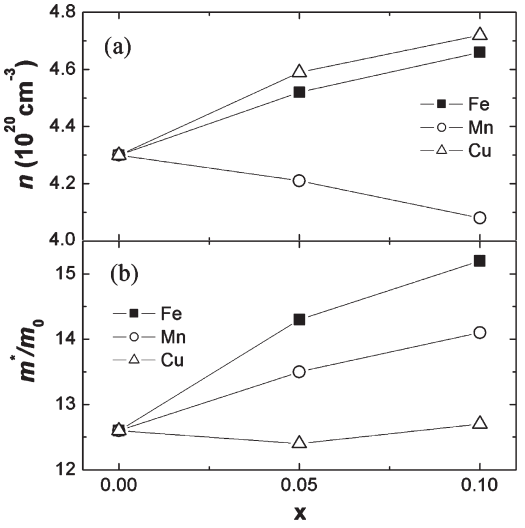

Figure 3. (a) Room-temperature carrier concentration n and (b) effective mass m^* as a function of doping level x for the samples; m_0 denotes the rest mass of electrons.

on oxygen content. From iodometric titration, the average valence of Co is higher than that of Fe and Cu, but lower than that of Mn in these specimens. As the changes in oxygen content are slight, the variations of the average valence of the Co site should be attributed mainly to Fe/Mn/Cu doping, which can change the hole concentration in the system. The room-temperature carrier concentration n obtained by Hall measurements is shown in Figure 3a. One can see that Fe or Cu doping increases carrier concentration, while Mn doping decreases carrier concentration. Considering the valent characteristics of Fe and Cu ions that Fe can be Fe^{2+} or Fe^{3+} and Cu is usually Cu^{2+}, of which the valences are all lower than the average valence of Co in $Ca_3Co_4O_9$, hence the substitution of Fe or Cu for Co is "hole-doping" that introduces hole carriers and thus results in the decrease of ρ. For Mn doping, although Mn ions may be Mn^{2+}, Mn^{3+}, or Mn^{4+}, the fact that the substitution of Mn for Co decreases n of the system suggests that Mn^{4+} should be dominant because the average valence of Mn is higher than that of Co (i.e., "electron-doping"), so ρ increases consequently. Herein the change in ρ with Mn doping is similar with the previous reports.[20,25] In addition, we notice that ρ of our $Ca_3Co_4O_9$ ceramic is about four times larger than that of single crystals or epitaxial films,[11,27] which most likely results from the porous microstructure and a large grain boundary scattering of carriers in these ceramic samples.

In general, S of the $Ca_3Co_4O_9$ system can be expressed by the Mott formula (originating from the Sommerfeld expansion).[21,28] By substituting $\sigma = en\mu(\varepsilon)$, one can obtain

$$S(T) = \frac{c_e}{n} + \frac{\pi^2 {k_B}^2 T}{3e}\left[\frac{\partial \ln \mu(\varepsilon)}{\partial \varepsilon}\right]_{\varepsilon=\varepsilon_F} \quad (1)$$

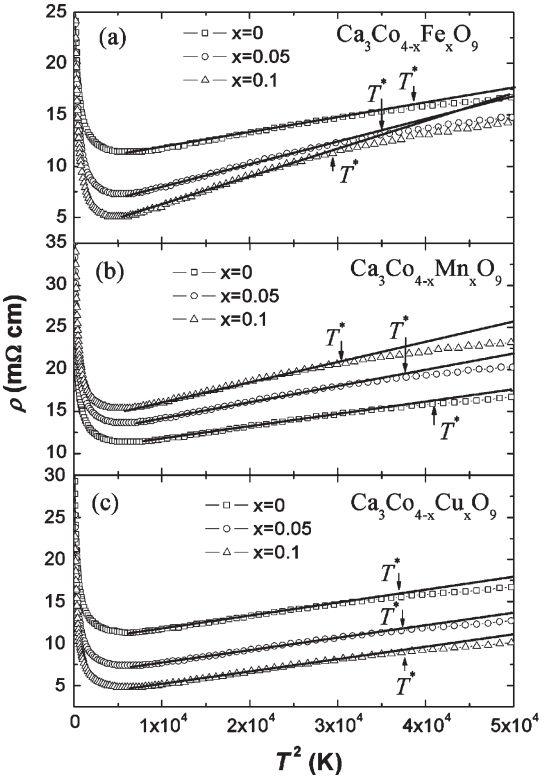

Figure 4. Variations of ρ versus T^2 for the three series. The solid lines are linear fitting using $\rho = \rho_A + AT^2$. The transition temperature T^* is marked by arrows.

where n, $\mu(\varepsilon)$, c_e, and k_B are carrier concentration, energy correlated carrier mobility, electronic specific heat, and Boltzmann constant, respectively. Usually, the first term of eq 1 is dominant, which is similar with the simple Drude picture $S \sim c_e/n$,[29] so the change in S can mostly be explained by the variation of carrier concentration n.[21,30] At present, it seems that the Drude picture can indeed elucidate that Mn doping reduces n and thus enhances S, and Cu doping increases n and hereby reduces S. However, the case of Fe doping cannot be explained by this scenario because of the simultaneous increase of n and S. Furthermore, the enhancement of S with Mn doping cannot be quantitatively explained by this scenario. Apparently, other factors must be considered to clarify these issues. Since the electronic correlation plays an essential role in S of $Ca_3Co_4O_9$, next we focus on the strongly correlated properties of this system.

As reported previously,[11] there are two characteristic temperatures in $Ca_3Co_4O_9$ between 5 K and 300 K, T_{MI} and T^*, where T_{MI} is the MI transition temperature and T^* is the transition temperature from Fermi liquid to incoherent metal. In the temperature range between T_{MI} and T^*, $Ca_3Co_4O_9$ exhibits a strongly correlated Fermi liquid behavior with a resistivity variation as $\rho = \rho_A + AT^2$, where A is the Fermi liquid transport coefficient.[11] All the $Ca_3Co_{4-x}M_xO_9$ samples exhibit such a temperature region as shown in Figure 4. The values of T_{MI} and

(27) Sugiura, K.; Ohta, H.; Nomura, K.; Hirano, M.; Hosono, H. *Appl. Phys. Lett.* **2006**, *89*, 032111.
(28) Fisher, B.; Patlagan, L.; Reisner, G. M.; Knizhnik, A. *Phys. Rev. B* **2000**, *61*, 470.
(29) Aschcroft, N. W.; Mermin, N. D. *Solid State Physics*; HoltSaunders: Philadelphia, PA, 1976.
(30) Liu, H. Q.; Song, Y.; Zhang, S. N.; Zhao, X. B.; Wang, F. P. *J. Phys. Chem. Solids* **2009**, *70*, 600.

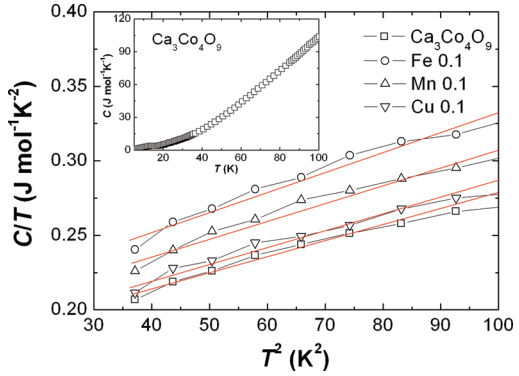

Figure 5. Temperature dependence of specific heat C for the samples plotted as C/T versus T^2 with the fitted lines. The inset displays C versus T for $Ca_3Co_4O_9$.

T^* are listed in Table 1. Here T_{MI} is determined as the temperature at which the slope $d\rho/dT$ is zero in $\rho-T$ curves, and T^* is defined as the end temperature of the linear dependence for $\rho \sim T^2$. A remarkable feature of the fitting results is the systematic decrease of T_{MI} and T^* and the increase of slope A for Fe or Mn doped samples, whereas T_{MI}, T^*, and A all keep nearly unchanged for Cu doped samples. Although the estimated magnitudes of A for all the samples are comparable to heavy fermion compounds, the variations of A and the transition temperatures suggest that the electronic correlation is indeed changed by Fe or Mn doping.

According to the dynamical mean field theory (DMFT),[31] a key role of effective mass m^* of a Fermi liquid is predicted as $T^* \sim 1/m^*$ and $A \sim (m^*)^2$. The decrease of T^* along with the increase of A indicates the increase of m^*. The notable increase of m^* in Fe or Mn doped samples (see Figure 3b and Table 1) implies a decreased bandwidth and an enhanced electronic correlation in these compounds. As for Cu doped samples, the electronic correlation (and the bandwidth) is nearly unchanged since the variation of m^* is quite small. To confirm the effects of M doping on m^* and electronic correlations, specific heat measurements were performed. Temperature dependence of specific heat C in low temperature range can be written as

$$C = \gamma T + \beta T^3 \tag{2}$$

in which γT and βT^3 denote the electron and lattice contribution to specific heat, respectively. By the linear fitting of $C/T \sim \gamma + \beta T^2$, one can obtain the electronic specific heat coefficient γ.[12] (Herein we ignore the magnetic specific heat, because the contribution of magnetic specific heat seems negligible and the obtained γ value from specific heat experiments under 9T magnetic fields is almost identical to that under the 0T field.[11]) As seen from Figure 5, the samples all have large γ values, revealing the existence of strong electronic correlations in the system. Fe and Mn doping increases γ, indicating the enhancement of m^* and electronic correlation, whereas Cu doping only induces a slight alteration of electronic correlation. These results are consistent with the resistivity measurements and further confirm the variations of electronic correlations by doping in this system. On the other hand, we should emphasize that the strongly correlated properties of this system are not eliminated by the Co-site doping. An evidence for this is the calculated quantity $A(T^*)^2/b_2$, where b_2 is the in-plane lattice parameter of CoO_2 subsystem. The values of $A(T^*)^2/b_2$ remain constant in the main and of order h/e^2 for all samples, implying the strongly correlated nature in these compounds. Also, the estimated Kadowaki−Woods ratios A/γ^2 are all $\sim 10^{-5}$ $\mu\Omega$ cm $K^2/(mJ^2\ mol^{-2})$, in good agreement with the values of Fermi liquid.[32] Additionally, it should be noted that the results herein can be compared with high-pressure studies on $Ca_3Co_4O_9$.[11] Pressure induces a decrease of transport coefficient A together with an increase of T^*, due to the increase of bandwidth under pressure. Hence, the correlations and effective mass are lowered by pressure, which is a typical behavior of strongly correlated Fermi liquid.[33]

Now we elucidate the unusual change in S in Fe doped samples. The substitution of Fe for Co dramatically increases the electronic correlation and effective mass; namely, the electronic specific heat is essentially enhanced. As a result, the increase of S due to the enhancement of electronic correlation exceeds the reduction of S resulting from the increase of carrier concentration, so overall S increases gradually with doping. For Mn doped samples, the increase of S arises partially from the decrease of hole concentration and partially from the enhancement of electronic correlation. Because Fe doping leads to more noticeable enhancement of electronic correlation than Mn, the increment of S in the Fe doped series is larger than the Mn doped series in the case of same doping level. This result also demonstrates the crucial role of electronic correlation in determining S in such strongly correlated electron systems. As for Cu doped series, on account of its nearly unaltered electronic correlation, S lessens normally as the hole density increases with doping.

To validate the effects of electronic correlation on S mentioned above, we also relate thermopower to effective mass directly on the basis of Boltzmann transport model.[34] In this model, one can solve the Boltmann equation and drive the following expression for thermopower,

$$S = \frac{k_B}{e}\left[\frac{(r+5/2)F_{r+3/2}(\zeta_F)}{(r+3/2)F_{r+1/2}(\zeta_F)} - \zeta_F\right] \tag{3}$$

and the carrier density n can be expressed by

$$n = 4\pi\left(\frac{2k_B m^* T}{h^2}\right)^{3/2} F_{1/2}(\zeta_F) \tag{4}$$

(31) Georges, A.; Kotliar, G.; Krauth, W.; Rozenberg, M. J. *Rev. Mod. Phys.* **1996**, *68*, 13.
(32) Kadowaki, K.; Woods, S. B. *Solid State Commun.* **1986**, *58*, 507.
(33) Limelette, P.; Wzietek, P.; Florens, S.; Georges, A.; Costi, T. A.; Pasquier, C.; Jérome, D.; Mézière, C.; Batail, P. *Phys. Rev. Lett.* **2003**, *91*, 016401.
(34) Durczewski, K.; Ausloos, M. *Phys. Rev. B* **2000**, *61*, 5303.

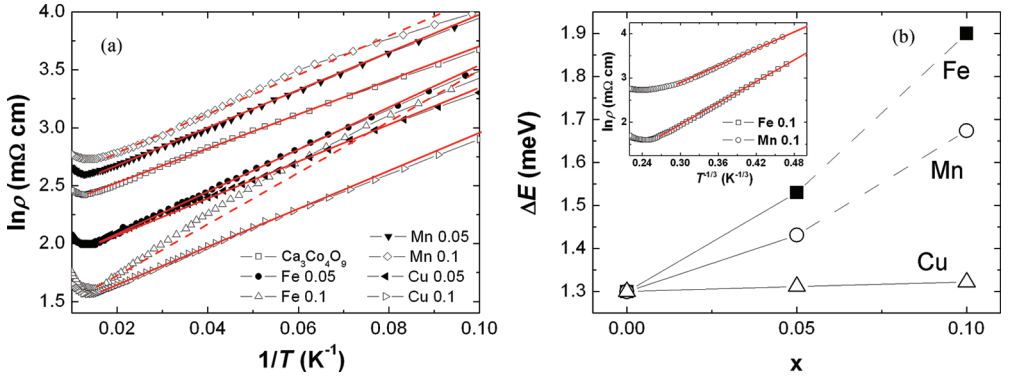

Figure 6. (a) Fitting plot of $\rho-T$ curves according to thermally activated model and (b) obtained activation energy ΔE for the samples. Fe 0.1 and Mn 0.1 samples cannot be well fitted by the thermally activated model, so their fitting lines are represented by broken lines. The inset of (b) shows the fitting plot of $\rho-T$ curves according to 2D-VRH model for Fe 0.1 and Mn 0.1 samples.

where r is scattering parameter, ζ_F is reduced chemical potential, $F_r(\zeta_F)$ is Fermi integral, and h is Planck constant. If we let $r = 3/2$ (ionized impurity scattering), as used for other cobaltites,[35] the values of m^* calculated based on the experimental S and n for all samples are comparable to those estimated values from the transport and specific heat measurements. When other r values are adopted, the doping level dependences of m^* are qualitatively similar to each other, although the magnitudes of m^* depend on the scattering parameter. Therefore, if we assume r is between 3/2 and 2 (it is reported that $r = 2$ is more suitable in titanates which have approximative m^* with $Ca_3Co_4O_9$[36]), S of all the samples can be well reproduced using the measured m^* and n values. These results indicate the close coupling of thermopower and electronic correlation, such that the unexpected enhancement of S can be ascribed to the variation of electronic correlation.

An additional evidence for the relationship between thermopower and electronic correlation is that the temperature dependence of S from ~20 K up to ~$2T^*/3$ can be described using a renormalized free electron thermopower S^* theory,[29] namely,

$$S(T) = S^*(T) + S_0 = \left(\frac{\pi^2}{6}\right)\frac{k_B T}{eT^*} + S_0 \qquad (5)$$

where S_0 is a constant thermopower. Figure 2b shows the linear relationship between S and T in this temperature range. Because of the proportionality between S^* and the inverse of T^*, the slope of the $S-T$ curves within such a temperature range will increase if the electronic correlation is enhanced. As displayed in Figure 2b, it is clear that the slope of fitting solid lines increases by Fe or Mn doping (and the slope of the Fe doped sample is larger than that of the Mn doped sample) but does not show detectable variation by Cu doping. In this temperature range, S also agrees with $S(T) = (\gamma/c)T + S_0$,[29] in which c is a parameter. The increase of slope by Fe of Mn doping reflects the enhancement of γ, corresponding to the aforementioned specific heat evidence. The deviation from linearity below 20 K may be due to the absence of spin degree of freedom of Co ions.[14] If we also linearly fit $S-T$ above T^* and define T_S^* as the cross point of the two straight lines (marked by arrows in Figure 2b), one can see that the evolution of T_S^* is also consistent with T^* and T_{MI}. The physical meaning of T_S^* and the relationship among T_S^*, T^*, and T_{MI} are not clear at this stage, but the identical evolution of T_S^*, T^*, and T_{MI} suggests that they may have the same origin.

Transport Mechanism and Magnetic Properties. To explore the reason for the distinct variations in strongly correlated properties induced by Fe/Mn doping and Cu doping, now we look at the transport mechanism and magnetic properties of this system. It is well-known that in the low temperature insulator-like state the variation of ρ with T of $Ca_3Co_4O_9$ obeys the thermally activated behavior,[5,20,21]

$$\rho = \rho_0 \exp\left(\frac{\Delta E}{k_B T}\right) \qquad (6)$$

where ρ_0 is a preexponential factor and ΔE is the activation energy. As seen from Figure 6a, $\rho-T$ of pure $Ca_3Co_4O_9$ and all the Cu doped samples can be well fitted by the activation model, and $\rho-T$ of Fe, Mn $x = 0.05$ doped samples can be mainly fitted by this model. This indicates the thermally activated transport mechanism in these compounds. However, $\rho-T$ of Fe, Mn $x = 0.1$ doped samples does not follow eq 6 well. If we disregard the deviation from exponential law of Fe, Mn $x = 0.1$ doped samples and fit all data using eq 6, one can find from Figure 6b that the obtained activation energy ΔE increases evidently for Fe and Mn doped series but remains nearly unchanged for Cu doped series.

In fact, $\rho-T$ of Fe, Mn $x = 0.1$ doped samples can be well fitted by the Mott's two-dimensional variable range hopping (2D-VRH) model. According to VRH theory,[37]

(35) Iwasaki, K.; Ito, T.; Nagasaki, T.; Arita, Y.; Yoshino, M.; Matsui, T. *J. Solid State Chem.* **2008**, *181*, 3145.
(36) Okuda, T.; Nakanishi, K.; Miyasaka, S.; Tokura, Y. *Phys. Rev. B* **2001**, *63*, 113104.
(37) Mott, N. F.; Davis, E. A. *Electronic Processes in Non-Crystalline Materials*; Clarendon: Oxford, 1979.Mott, N. F. *Metal-Insulator Transitions*; Taylor and Francis: London, 1990.

the relationship between resistivity and temperature in a 2D system is written as

$$\rho = \rho_0' \exp\left(\frac{T_0}{T}\right)^{1/3} \quad (7)$$

where ρ_0' is a constant, $T_0 = 8/[\pi k_B N(\varepsilon_F) l_v^2]$ is the VRH characteristic temperature associated with the density of localized states at Fermi energy $N(\varepsilon_F)$, and l_v is localization length. As shown in the inset of Figure 6b, the linear relationship of ln ρ versus $T^{-1/3}$ indicates the transport mechanism of Fe, Mn $x = 0.1$ doped samples has turned into 2D-VRH. Such results are reminiscent of the behavior found in Co-site doped $NaCo_2O_4$ in which there is only one kind of Co site: the CoO_2 layer.[38,39] The transport properties in the Fe/Mn doped series vary in a similar way with those of Co-site doped $NaCoO_2$, but the behaviors of Cu doped $Ca_3Co_4O_9$ are highly incompatible with that reported in $NaCo_{1-x}Cu_xO_2$. Consequently, it should to be explained that Fe and Mn substitute for the Co sites in CoO_2 layers whereas Cu substitutes for the Co sites in Ca_2CoO_3 layers.

The on-resonant spectra of X-ray photoemission spectroscopy (XPS) for $Ca_3Co_4O_9$ reveals that Co 3d partial density of states in Ca_2CoO_3 layers hardly reaches the Fermi level,[40] which indicates that Co ions in Ca_2CoO_3 layers have very limited effects on the transport properties. In contrast, the Fermi energy lies in the crystal-field gap of the d states in CoO_2 layers,[23] so Co ions in CoO_2 layers dominate the transport properties. In another words, the substitutions for Co sites in different sublayers will lead to two distinct transport behaviors. For Cu doping, the substitution of Cu for Co in Ca_2CoO_3 layers has little influence on the transport mechanism, so that the activation energy also remains unchanged. However, the substitution of Fe/Mn for Co takes place in CoO_2 layers, which can not only produce potential disorder that enhances the thermal activation energy but also gradually change the transport mechanism because the conduction path in CoO_2 layers is disturbed. If strong distortions and disorder in CoO_2 layers are induced by heavier doping, the hole hopping tends toward farther low-energy sites, and then VRH mechanism dominates. This is just the case of Fe and Mn $x = 0.1$ doped samples. Moreover, due to the anisotropic layered structure of $Ca_3Co_4O_9$ system, the VRH mechanism of the two samples is two-dimensional, rather than the usual three-dimensional as found in isotropic semiconductors. In this 2D-VRH framework, the fitted values of T_0 are 537.6 K and 291.3 K for Fe 0.1 and Mn 0.1, respectively. Generally, the variation of state density at the Fermi surface with carrier concentration is not strong. Then assuming the density of localized states $N(\varepsilon_F)$ to possess a reasonable value of 10^{20} cm^{-3} eV^{-1},[20] the plane density of states at the Fermi level (in the CoO_2 layer) can be deduced to be $\sim 10^{13}$ cm^{-2} eV^{-1}.[37,41] (The detailed estimation process can be found in refs 41 and 37, Chapters 1 and 2.) Subsequently, one can estimate the localization length $l_v \sim 22$ nm and ~ 29 nm for Fe 0.1 and Mn 0.1, respectively. These localization length values suggest that holes in Fe doped samples are more localized than Mn doped samples, consistent with that the Fe doped series have higher activation energy (see Figure 6b).

It should be noted that the different M doping sites also influence IC-SDW transition. The positive muon spin rotation and relaxation (μ^+SR) experiments confirm that the IC-SDW is not likely to be caused by the misfit between the two sublayers but is an intrinsic behavior of CoO_2 layers.[16] The emergence of IC-SDW ordering localizes hole carriers and thus gives rise to the MI transition;[15,16] in other words, the IC-SDW transition is coherent to this MI transition. As listed in Table 1, T_{MI} decreases by Fe or Mn doping, suggesting that the IC-SDW transition in these samples occurs in lower temperatures than undoped $Ca_3Co_4O_9$. For the Cu doped series, the IC-SDW transition does not show obvious variation. Although the average valences of Co in the three series are all changed by Fe, Mn, or Cu doping, we can conclude that IC-SDW transition is possibly dependent on the average valences of Co ions in CoO_2 layers rather than that of total Co ions in this system.

Such differences in transport properties by M doping can also be reflected in their magnetic properties. Figure 7 shows the temperature dependences of magnetic susceptibility χ and magnetic field dependences of magnetization at 5 K M_{5K} of the samples. One can see that χ increases monotonically with decreasing temperature. χ sharply increases as temperature further decreases from $\sim$19 K, which is suggested to be a ferrimagnetic transition.[14] The values of χ for Fe/Mn doped samples are lower than for the undoped one, indicating that the ferrimagnetism is suppressed by Fe or Mn doping. As reported previously, the ferrimagnetism is caused by the interlayer coupling between CoO_2 and Ca_2CoO_3 subsystems, and superexchange and double exchange interactions coexist between Co^{3+} and Co^{4+} in CoO_2 layers.[2,14−16] Fe or Mn doping in CoO_2 layers will introduce Co^{4+} or Co^{3+} based on valence equilibrium. In both cases, the interlayer coupling will be disturbed and the superexchange interaction will be enhanced, so the suppression of ferrimagnetism can be anticipated. As for Cu doping, considering the structural feature of the Ca_2CoO_3 layer that consists of two Ca−O planes and one Co−O plane, where the Co−O plane is sandwiched by the two Ca−O planes,[2] a small amount of doping into the inner Co−O planes hardly affects the magnetic and transport properties. Therefore, the ferrimagnetism is not suppressed by Cu doping; also, the

(38) Ito, M.; Nagira, T.; Oda, Y.; Katsuyama, S.; Majima, K.; Nagai, H. *Mater. Trans.* **2002**, *43*, 601.
(39) Terasaki, I.; Ishii, Y.; Tanaka, D.; Iguchi, Y. *Jpn. J. Appl. Phys.* **2001**, *40*(Part 2), L65.
(40) Takeuchi, T.; Kondo, T.; Takami, T.; Takahashi, H.; Ikuta, H.; Mizutani, U.; Soda, K.; Funahashi, R.; Shikano, M.; Mikami, M.; Tsuda, S.; Yokoya, T.; Shin, S.; Muro, T. *Phys. Rev. B* **2004**, *69*, 125410.
(41) Lisunov, K. G.; Raquet, B.; Rakoto, H.; Broto, J. M.; Arushanov, E.; Xu, X. Z.; Alami, H. E.; Cavellin, C. D. *J. Appl. Phys.* **2003**, *94*, 5912.

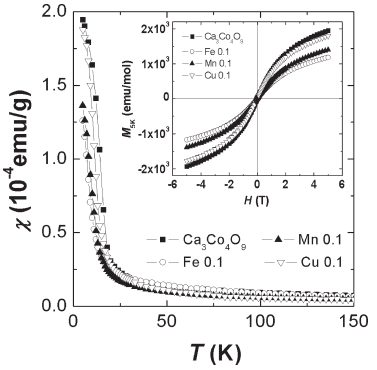

Figure 7. Temperature dependence of magnetic susceptibility χ of the samples. The inset shows the $M_{5K}-H$ plot. We mention that only a very weak hysteresis in the $M_{5K}-H$ curve was observed in our ceramic samples. The coercive field is ~50 Oe. This result is similar with the observed $M_{ab}-H$ of single crystal $Ca_3Co_4O_9$ (see ref 14).

transport mechanism and IC-SDW transition are not influenced. The $M_{5K}-H$ curves also reveal the variations of ferrimagnetism by M doping clearly (see the inset of Figure 7). Figure 8 plots $d\chi/dT-T$ curves, from which two characteristic temperatures T_1 and T_2 can be defined by linear fitting.[21] Both T_1 and T_2 may be related to the IC-SDW transition or magnetic transition.[21] Similar with T_{MI} and T^*, T_1 and T_2 both shift to lower temperatures in Fe and Mn doped series, which may again suggest that the effects of M doping on electronic correlation, transport, and magnetic properties are relevant to each other.

Next, a question of concern is why the substitution of Fe/Mn for Co takes place in CoO_2 layers whereas the substitution of Cu takes place in Ca_2CoO_3 layers. A possible reason is because of their different ionic radii. Considering the usual spin states of these cations (including high spin state, intermediate spin state, or low spin state, abbreviated to HS, IS, and LS, respectively), the radii in six-coordination of Fe^{2+} (0.61 Å LS) and Fe^{3+} (0.55 Å LS) and Mn^{3+} (0.645 Å HS) and Mn^{4+} (0.53 Å HS) are very close to those of Co^{3+} (0.545 Å LS) and Co^{4+} (0.53 Å HS) according to Shannon's Table.[42] This means that Fe or Mn ions can be easily substituted for Co ions in CoO_2 layers. As for Cu^{2+}, its radius (0.73 Å) is much larger than the radii of Co^{3+}or Co^{4+} but close to Co^{2+} (0.745 Å HS, and Co^{2+} is always a HS ion[43]) in Ca_2CoO_3 layers. Therefore, Cu ions are hardly doped in CoO_2 layers, but it is easier to replace the Co ions in Ca_2CoO_3 layers. Nevertheless, more unambiguous evidence for the reason why Fe/Mn and Cu exist in different sublayers needs further study.

$Ca_3Co_4O_9$ and $NaCo_2O_4$ have the same CoO_2 layers, and both exhibit unusual large thermopower, implying the strong interactions between 3d electrons in CoO_2 layers. That is to say, the CoO_2 layers are crucial in the electronic correlations. Accordingly, the variations (electronic state, disorder, distortions, etc.) of CoO_2 layers induced by Fe and Mn doping will change the band structure, which may conduce to the enhanced

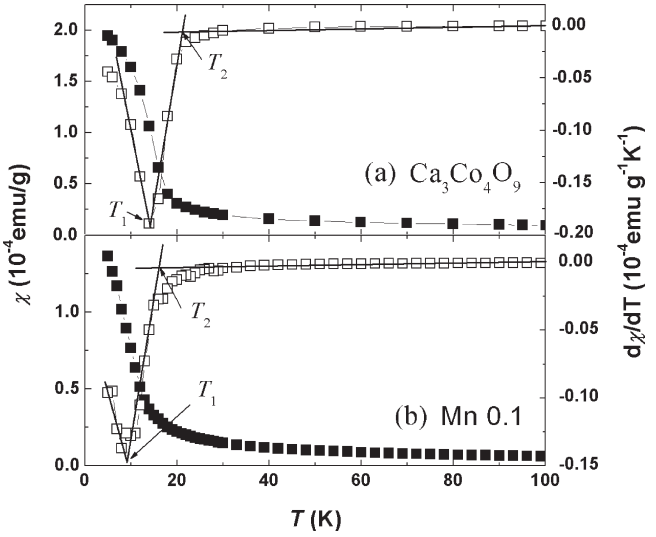

Figure 8. Temperature dependence of magnetic susceptibility χ (solid squares) along with its slope $d\chi/dT$ (open squares) for (a) $Ca_3Co_4O_9$ and (b) Mn 0.1 sample. The two variations in $d\chi/dT$ versus T curves are signaled by T_1 and T_2.

electronic correlations as a result. On the other hand, compared with Fe, the radii of Mn ions are closer to those of Co ions in CoO_2 layers, so the substitution of Fe for Co will bring on stronger structural distortions than Mn (this is also evidenced by the larger activation energy ΔE in Fe doped series). Analogous to perovskite-type cobaltites such as $LaCoO_3$ that has similar CoO_6 lattices with the CoO_2 layer in $Ca_3Co_4O_9$,[35] Fe doped samples can have smaller Co−O−Co bond angles and hopping integral because of their larger distortions. This will narrow the bandwidth. Therefore, Fe doping can induce a more prominent enhancement of electronic correlation than Mn in this system. This explains why the Fe doped series exhibits more remarkable increase in thermopower and more pronounced variations of the characteristic parameters (T_{MI}, T^*, T_S^*, A, etc.). The CoO_2 layers are not affected in Cu doped series, so the electronic correlations and characteristic parameters are not changed in these Cu doped samples.

Thermoelectric Properties. Since the resistivity and thermopower of $Ca_3Co_4O_9$ both vary by M doping, we now test whether the thermoelectric characteristics are improved. The temperature dependence of thermal conductivity κ of the samples is shown in Figure 9. One can see that the shapes of the $\kappa-T$ curves are similar, but the values of κ decrease with doping (see Table 1). In general, κ can be expressed as a sum of phonon thermal conductivity term κ_{ph} and the carrier thermal conductivity term κ_{car}, namely, $\kappa = \kappa_{ph} + \kappa_{car}$. From the estimation by Wiedemann−Franz's law, phonon thermal conductivity κ_{ph} is the predominant component in κ of all the specimens, so the variation of κ mainly originates from the change in κ_{ph}. Because the doped M ions as defects can cause disorder and structural distortion, the induced lattice disharmony will scatter phonons, so the phonon transport will be suppressed and thus κ decreases. The most pronounced reduction of κ in the Cu doped series may originate from the largest weight of the Cu ion.

(42) Shannon, R. D. *Acta Crystallogr.* **1976**, *A32*, 751.
(43) Maignan, A.; Caignaert, V.; Raveau, B.; Khomshii, D.; Sawatzky, G. *Phys. Rev. Lett.* **2004**, *93*, 026401.

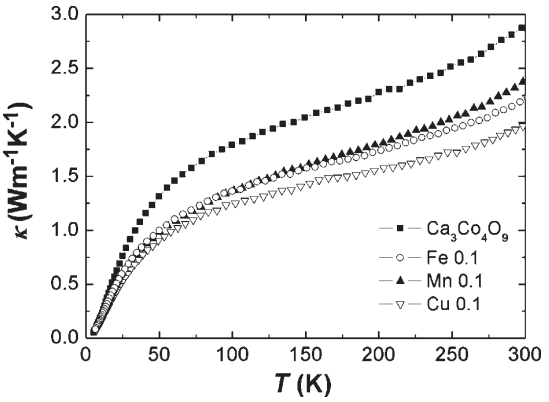

Figure 9. Temperature dependence of thermal conductivity κ of the samples.

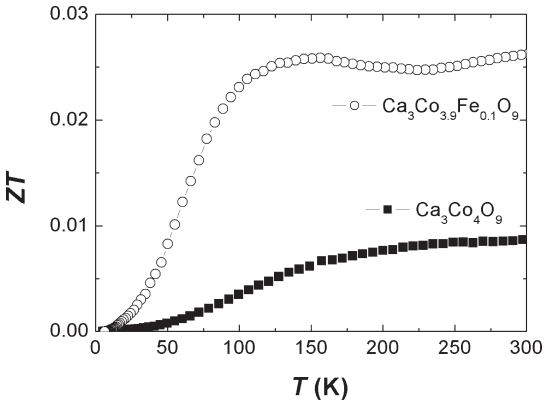

Figure 10. Temperature dependence of ZT of $Ca_3Co_4O_9$ and $Ca_3Co_{3.9}Fe_{0.1}O_9$.

Using the measured ρ, S, and κ, we can calculate the thermoelectric figure of merit ZT (defined by $ZT = S^2T/\rho\kappa$) of the samples. As listed in Table 1, although different M ions doping may induce either simultaneous increase or simultaneous decrease of ρ and S, the power factor P ($= S^2/\rho$) and ZT are both enhanced by doping. In addition, the suppression of κ with doping is also beneficial to the enhancement of ZT. A special case is the Fe doped series. As a result of the increase of S together with the reduction in ρ, the thermoelectric performance is improved notably by Fe doping. Figure 10 shows the temperature dependence of ZT values of $Ca_3Co_4O_9$ and $Ca_3Co_{3.9}Fe_{0.1}O_9$. It can be found that the ZT of $Ca_3Co_{3.9}Fe_{0.1}O_9$ is three times larger than that of the undoped sample up to 300 K. It is also noteworthy that after a slight concave around 230 K, the ZT value keeps a gradual increase to room temperature, suggesting it can reach its maximum above room temperature, so the compound may be a promising thermoelectric oxide for high temperature application.

A conclusion from these results is that thermoelectric performance of the $Ca_3Co_4O_9$ system can be improved efficiently by choosing suitable ions as dopants. The promising approach is to choose such doped ions that can evidently enhance electronic correlations and meanwhile introduce carriers. Although the largest ZT value obtained in this study is still much less than the applied criterion ($ZT \geq 1$), one can expect that codoping or suitable element addition may improve thermoelectric characteristics of this system further.[18,44] In fact, the relatively low ZT in this study can be partly attributed to the high resistivity. Since it is reported that high-textured $NaCo_2O_4$ and $Ca_3Co_4O_9$ specimens exhibit much lower resistivity than common ceramics,[26,45] using the hot-pressure technique, magnetic alignment technique, template growth method, and so forth to obtain highly grain-aligned ceramics is also a feasible way to improve the thermoelectric performance of this system.

Conclusions

Detailed investigations on the strongly correlated, electrical transport, and magnetic properties of Fe, Mn, and Cu doped $Ca_3Co_4O_9$ reveal that Fe/Mn substitute for Co in CoO_2 layers while the substitution of Cu for Co occurs in Ca_2CoO_3 layers. As a result, the electronic correlations of the system are enhanced remarkably by Fe and Mn doping, evidenced by the increase of effective mass, electronic specific coefficient, and the variations of some characteristic parameters and transition temperatures. Also, with Fe and Mn doping, the transport mechanism in low temperature insulator-like range varies from thermal activation to 2D-VRH gradually, and the ferrimagnetism is suppressed. As for the Cu doped series, the electronic correlation, transport, and magnetic properties all remain unaltered. The unusual increase of S in Fe doped samples can be well explained by the enhancement of electronic correlation, even if the carrier concentration is increasing with Fe doping. For these three doped series, the thermoelectric ZT values are all improved. Among them, the $Ca_3Co_{4-x}Fe_xO_9$ series exhibits the best thermoelectric performance, as a result of the simultaneous increase of S and decrease of ρ by Fe doping. This study proposes a likely strategy to further improve the thermoelectric characteristics of $Ca_3Co_4O_9$ and potentially other electron strongly correlated thermoelectric systems.

Acknowledgment. This work is supported by the start-up funding from Nanyang Technological University to H.J.F. and the National Natural Science Foundation of China (Grant Nos. 50672019 and 10804024).

Supporting Information Available: SEM image of the SEM micrograph of $Ca_3Co_4O_9$ sample (PDF). This material is available free of charge via the Internet at http://pubs.acs.org.

(44) Xu, G. J.; Funahashi, R.; Shikano, M.; Matsubara, I.; Zhou, Y. Q. *Appl. Phys. Lett.* **2002**, *80*, 3760.
(45) Cheng, J. G.; Sui, Y.; Fu, H. J.; Lu, Z.; Wei, B.; Qian, Z. N.; Miao, J. P.; Liu, Z. G.; Huang, X. Q.; Zhu, R. B.; Wang, X. J.; Su, W. H. *J. Alloys Compd.* **2006**, *407*, 299.